## Supporting Information

# A High-Current Initiated Formation Strategy for Improved Cycling Stability of Anode-Free Lithium Metal Batteries

Kangning Cai[1,2,†], Mengtian Zhang[1,2,†], Geng Zhong[1,2], Guohuang Kang[1,2], Jie Biao[1,2], Chuang Li[1,2], Yanru Liu[1,2], Guangmin Zhou[1,2,*], Feiyu Kang[1,2,*], Yidan Cao[1,2,*]

[1] Shenzhen Geim Graphene Center, Institute of Materials Research, Shenzhen International Graduate School, Tsinghua University, Shenzhen 518055, China

[2] Tsinghua-Berkeley Shenzhen Institute, Shenzhen International Graduate School, Tsinghua University, Shenzhen 518055, China

† These authors were equal major contributors.

* Corresponding Authors:

yidancao@sz.tsinghua.edu.cn (Yidan Cao), fykang@sz.tsinghua.edu.cn (Feiyu Kang), guangminzhou@sz.tsinghua.edu.cn (Guangmin Zhou)

## Finite element simulation

Based on the COMSOL Multiphysics 6.0 software, we performed the finite element analysis for the nucleation and growth process of Li as well as the properties of diffuse double layer. The following are the simulation equations:

**1. Nucleation and growth process of Li**

**Mass transport**

In the electrolyte, the transfer of ions is driven by migration because of electric field and diffusion because of concentration gradient which are governed by the Nernst−Planck equation:

$$N_i = -D_i(\nabla c_{0,i} - \frac{z_i F c_{0,i}}{RT}\nabla\Phi)$$

Where $N_i$ is flux, $D_i$, $z_i$ and $c_{0,i}$ is the diffusion coefficient, charge and concentration of species $i$, respectively. $F$ is the Faraday's constant, $R$ is the ideal gas constant, $T$ is the Kelvin temperature and $\Phi$ is the electrolyte potential. Meanwhile, the ions in the electrolyte follows the equation of conservation of mass and charge:

$$\frac{\partial c_i}{\partial t} + \nabla \times N_i = 0$$

$$\sum_i z_i c_i = 0$$

Where $c_i$ is the concentration, $z_i$ is the valence of each species in the electrolyte.

**Charge transfer**

Basically, $Li^+$ are transported from the bulk solution to the anode surface then reduced to Li-atom, and at the interface of the electrolyte and the anode, the deposition process of $Li^+$ can be described as the simplified reaction:

$$Li^+ + e^- \leftrightarrow Li$$

The electrochemical behaviors of $Li^+$ at the electrode-electrolyte interface could be described by the famous Butler-Volmer equation:

$$i_{loc} = i_{ex}\left[\exp\left(\frac{\alpha_a F\eta}{RT}\right) - \exp\left(\frac{-\alpha_c F\eta}{RT}\right)\right]$$

Where $i_{loc}$ is the local current density, which could be used to quantify the local reaction rate. η is overpotential, $\alpha_a$ and $\alpha_c$ are the anodic and cathodic charge transfer coefficients, respectively, and $i_{ex}$ is exchange current density which is defined as the current density flowing equally in each direction at the reversible potential and can be used to characterize the ease of a reaction to occur, moreover, it is closely related to the electron transfer kinetics and the concentration gradient near the surface:

$$i_{ex} = i_e \prod_{i,v_j>0} \left(\frac{c_{Li^+}}{c_b}\right)^{\frac{\alpha_a v_j}{n_j}} \prod_{i,v_j<0} \left(\frac{c_{Li^+}}{c_b}\right)^{\frac{-\alpha_c v_j}{n_j}}$$

Therefore, the $i_{ex}$ is greatly influenced by the $\frac{c_{Li^+}}{c_b}$ which is also refers to the concentration gradient. Where $c_{Li^+}$ and $c_b$ is the concentration of $Li^+$ near the anode and in the bulk electrolyte, respectively, $i_e$ is the current density to represent the kinetics of electrons, $v_j$ is the stoichiometric coefficients, $n_j$ is the number of electrons transferred. and the $\eta$ is the overpotential.

Where $\phi_s$ and $\phi_l$ is the solid phase and liquid phase potential, respectively, $U_{eq}$ is the equilibrium potential of the reaction.

**Morphology evolution**

Based on the above equations, the $i_{loc}$ is closely related to the $Li^+$ concentration distribution and the overpotential at the anode surface. Therefore, boundary conditions near the substrate can be described as:

$$N_{Li^+} \cdot n = -\frac{i_0}{2F}[\exp\left(\frac{\alpha_a F\eta}{RT}\right) - \frac{c_{Li^+}}{c_0} exp(\frac{\alpha_c F\eta}{RT})]]$$

Where ***n*** is the normal vector of the boundary.

Due to the initial nucleation behaviors of Li are highly related to the overpotential. Specifically, we set a random distribution function to simulate the nucleation morphology, which consists with the law that the radius of the nucleation is inversely

proportional to the overpotential and the nucleation density is proportional to the cubic of the overpotential.

**2. Diffuse double layer**

Close to an electrode surface, ions in the electrolyte are attracted and repelled by unscreened excess charge on the electrode. This region is called the diffuse double layer. Its size is normally a few nanometers away from the electrode surface but significantly influence the properties of SEI. The following are the governing equation for simulating the diffuse double layer

The concentrations, $c_i$ of two ions of opposite charge (+1/-1) are solved for in the electrolyte phase. The fluxes of the ions are described by the Nernst–Planck equation, and the ions follow the law of conservation of mass and charge, which is consistent with the equations in the above. For the potential, the Poisson equation stats:

$$\nabla \cdot ( - \varepsilon \nabla \Phi) = \rho$$

where $\varepsilon$ is the permittivity and $\rho$ is the charge density. The charge density depends on the ion concentrations according to:

$$\rho = F(c_+ - c_-)$$

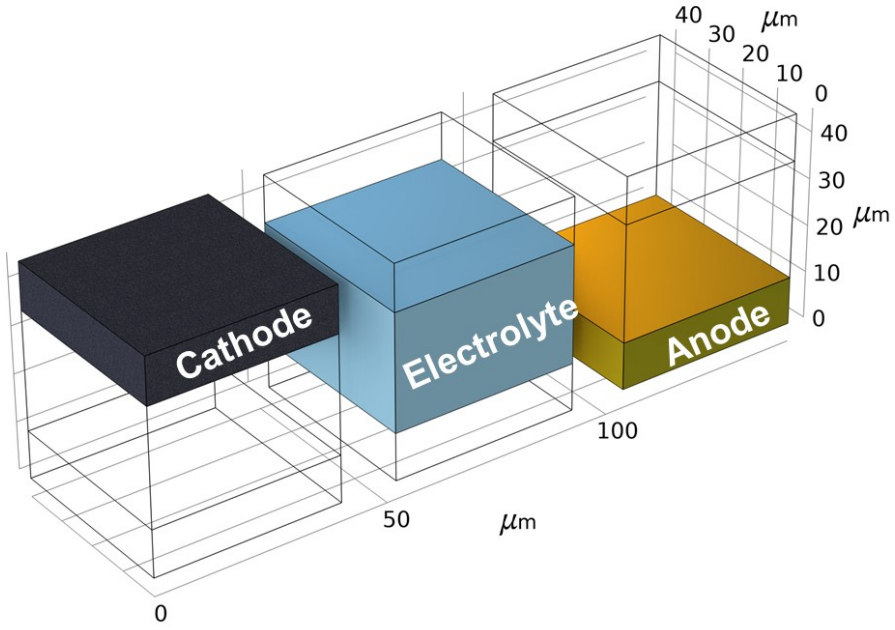


Figure S1. The geometry used for the FEM simulation.

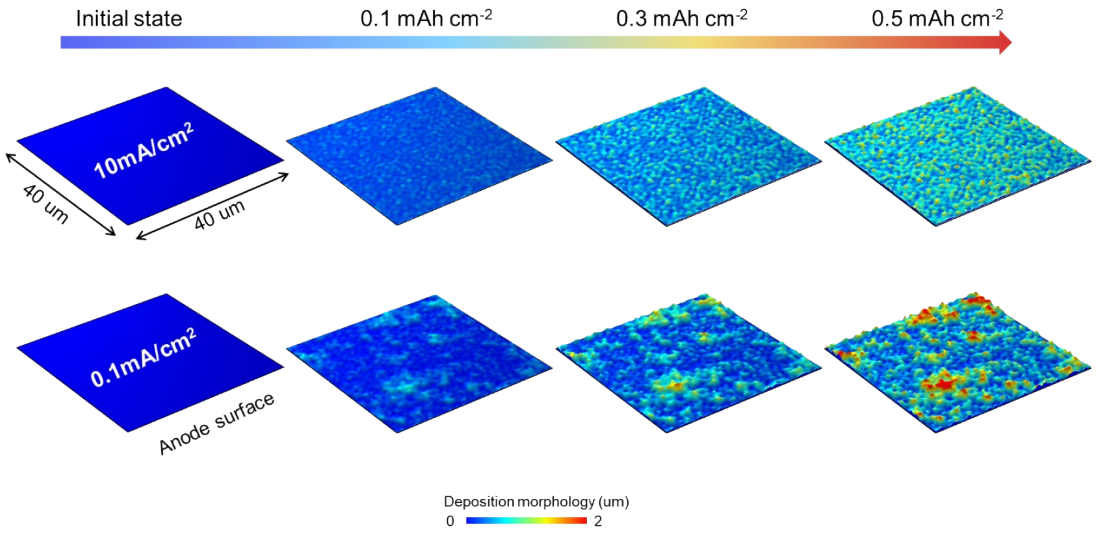


Figure S2. FEM simulation results for the anode morphology evolution of two different formation strategies.

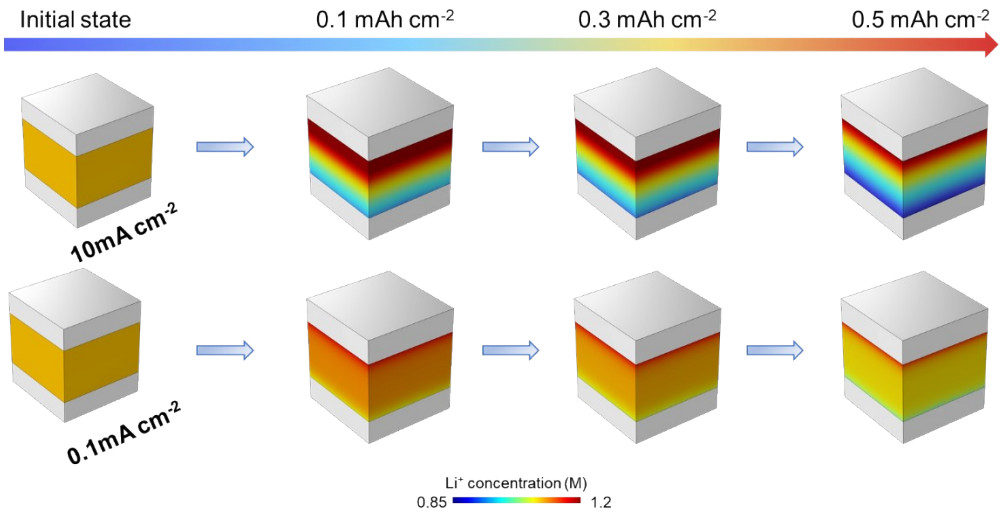


Figure S3. FEM simulation results for the $Li^+$ concentration evolution in the electrolyte of two different formation strategies.

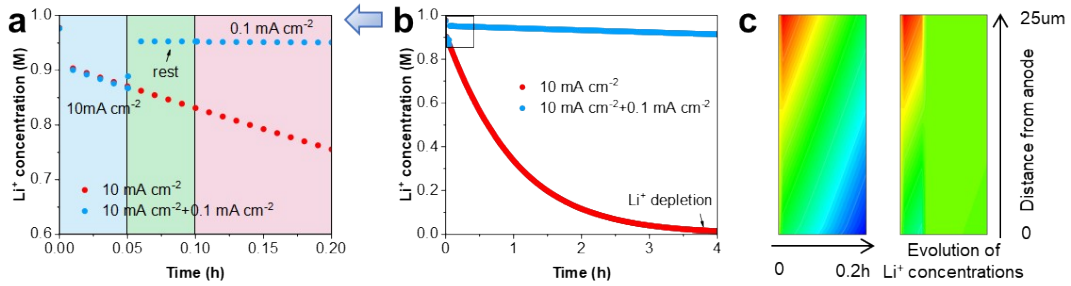


Figure S4. Comparison of $Li^+$ concentration evolution under two different charging models. (10 mA $cm^{-2}$ for 40 mAh $cm^{-2}$ and 10 mA $cm^{-2}$+0.1 mA $cm^{-2}$ for 40 mAh $cm^{-2}$)

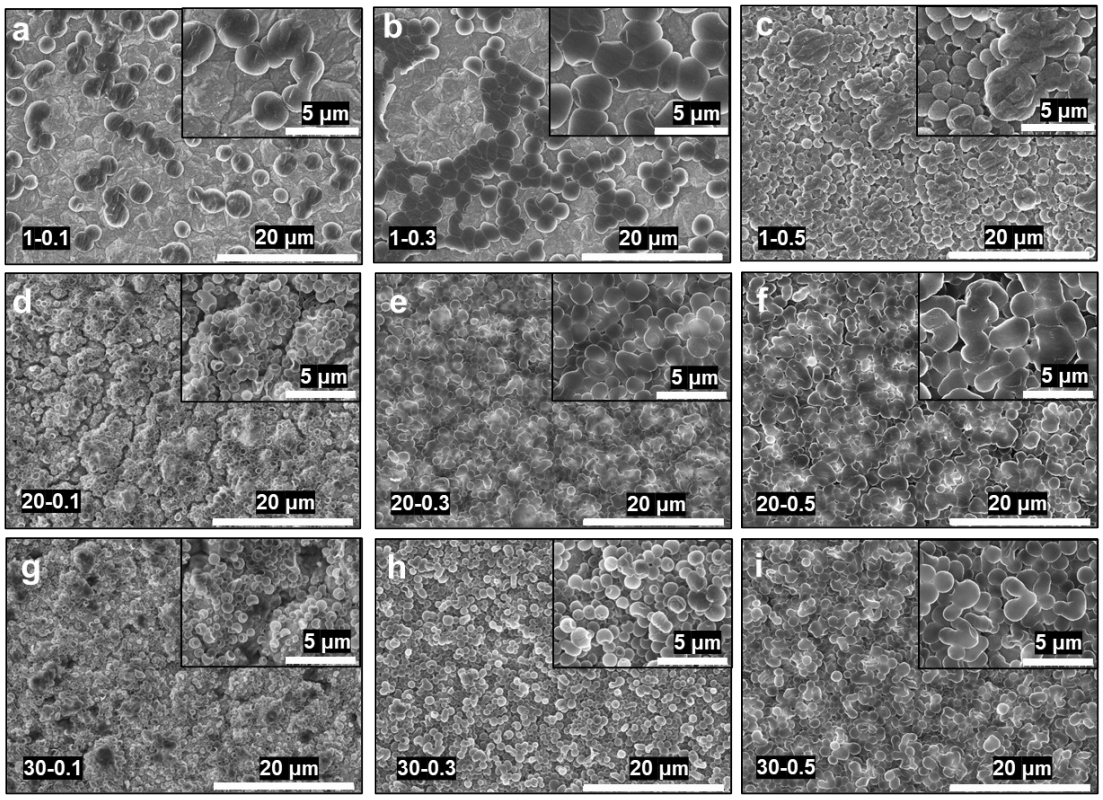


Figure S5. SEM images of Li nuclei layers at varied current densities with gradually increased deposition capacity. (denoted as current density-deposition capacity, eg, 1-0.1 represents that Cu substrate was deposited with lithium at the current density of 1 mA $cm^{-2}$ and areal capacity of 0.1 mAh $cm^{-2}$)

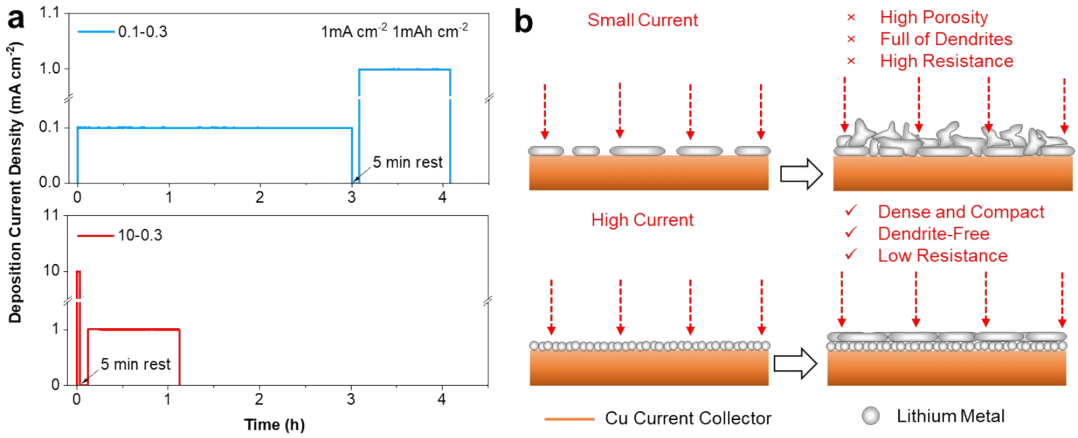


Figure S6. (a) Current vs time profiles for the two types of formation strategies. (b) Schematics of the Li nucleation and growth process under the two types of formation strategies.

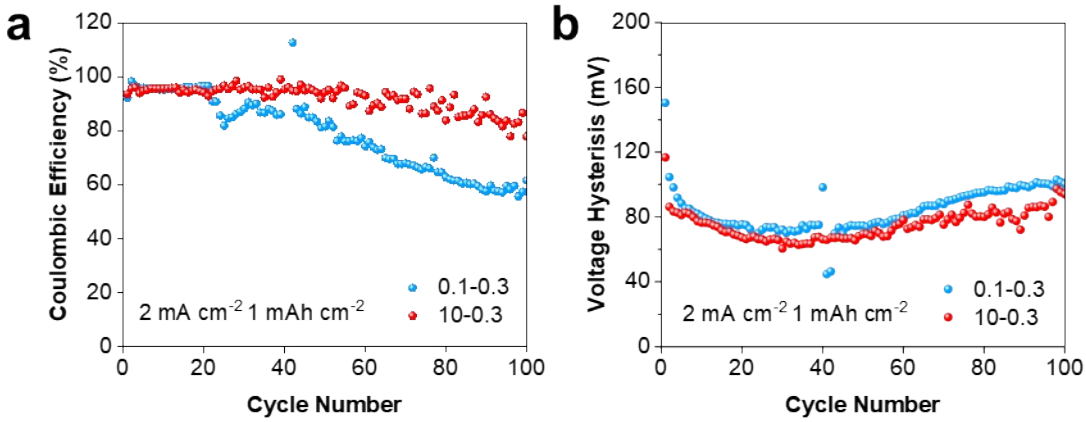


Figure S7. Comparison of (a) Li plating/stripping Coulombic efficiency (CEs) in Li||Cu cells which were plated at the current density of 0.1 mA $cm^{-2}$ and 10 mA $cm^{-2}$ with the capacity of 0.3 mAh $cm^{-2}$ and then cycled at the current density and capacity of 2 mA $cm^{-2}$ and 1 mAh $cm^{-2}$, and (b)corresponding voltage hysteresis.

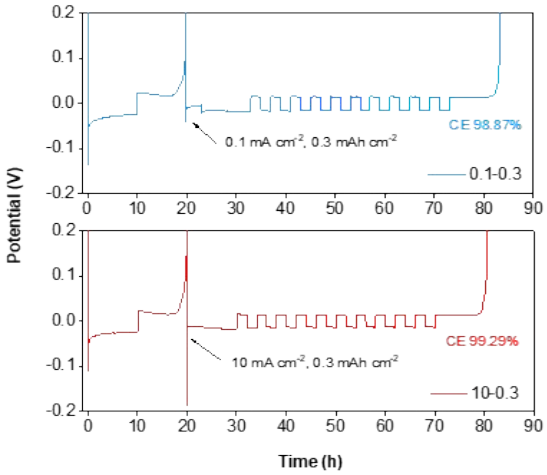


Figure S8. The modified Aurbach CE of Li plating/stripping after Li deposition at different current densities.

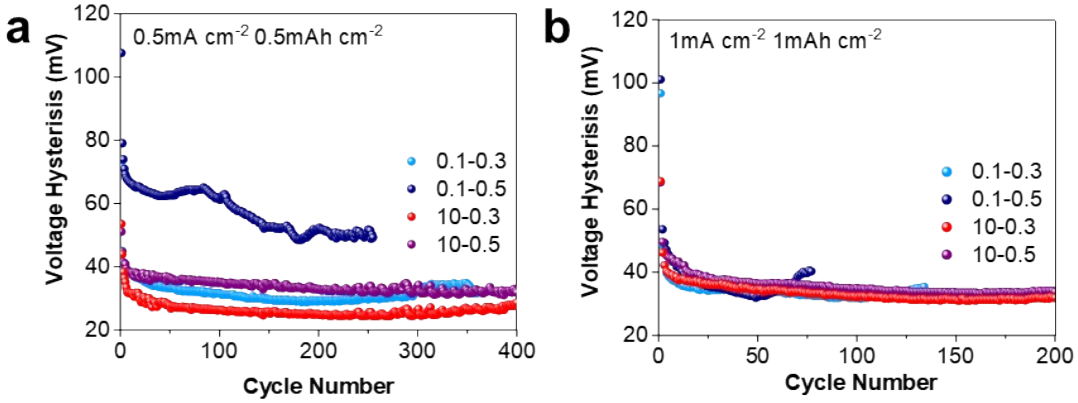


Figure S9. Corresponding voltage hysteresis of Li||Cu cells which were plated at the current density of 0.1 mA $cm^{-2}$ and 10 mA $cm^{-2}$ with the capacity of 0.3 mAh $cm^{-2}$ and 0.5 mAh $cm^{-2}$, and then cycled at (a) 0.5 mA $cm^{-2}$ and 0.5 mAh $cm^{-2}$, (b) 1 mA $cm^{-2}$ and 1 mAh $cm^{-2}$.

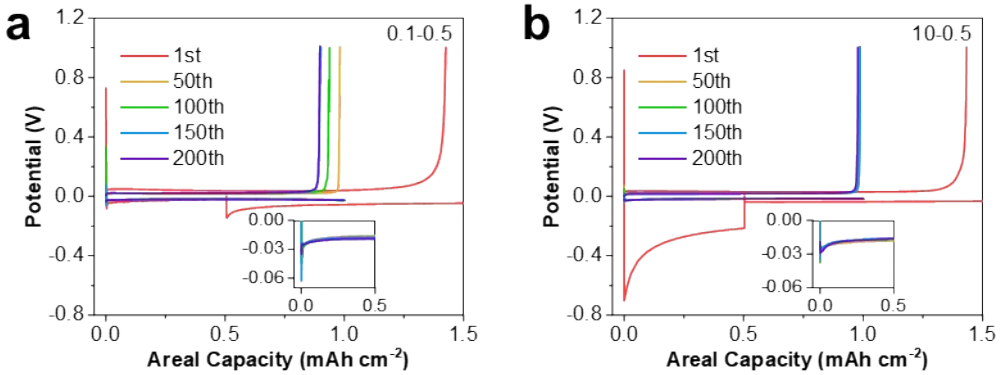


Figure S10. Galvanostatic charge–discharge curves of (a) 0.1-0.5 and (b) 10-0.5 cells at 1 mA $cm^{-2}$ and 1 mAh $cm^{-2}$ after 1, 50, 100, 150 and 200 cycles.

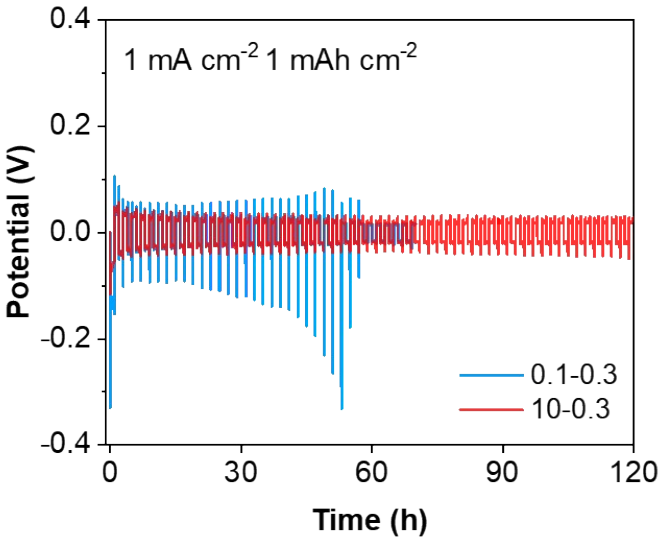


Figure S11. The voltage profiles of Li-Li symmetric cell at 1 mA $cm^{-2}$, 1 mAh $cm^{-2}$. The symmetric cells were assembled with two Cu foils which were plated at 0.1 mA $cm^{-2}$ or 10 mA $cm^{-2}$ for 0.3 mAh $cm^{-2}$ and then plated at 1 mA $cm^{-2}$ for 5 mAh $cm^{-2}$.

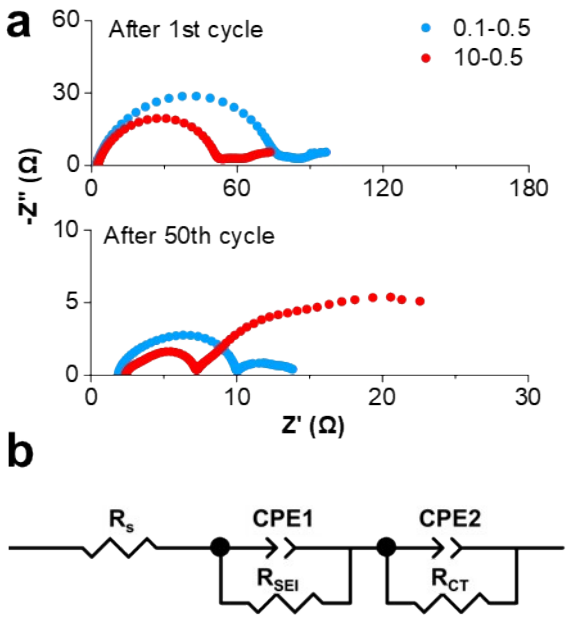


Figure S12. (a) Nyquist plots of 0.1-0.5 and 10-0.5 cells after 1 and 50 cycles at 1 mA $cm^{-2}$-1 mAh $cm^{-2}$, and (b) corresponding equivalent circuit model.

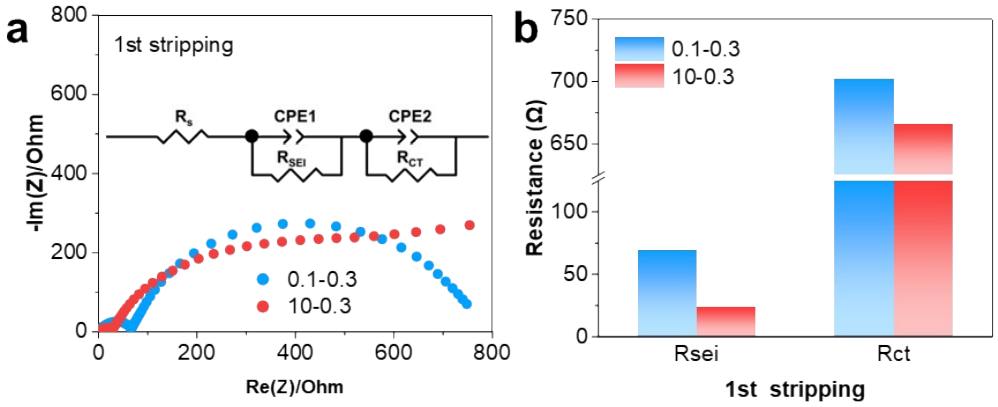


Figure S13. Electrochemical characteristics of 0.1-0.3 and 10-0.3 cells cycled at 1 mA $cm^{-2}$-1 mAh $cm^{-2}$. (a) Nyquist plots and (b) Calculated SEI resistance ($R_{SEI}$) and charge transfer resistance ($R_{CT}$) of Li||Cu cells after the 1st Li stripping to 1V.

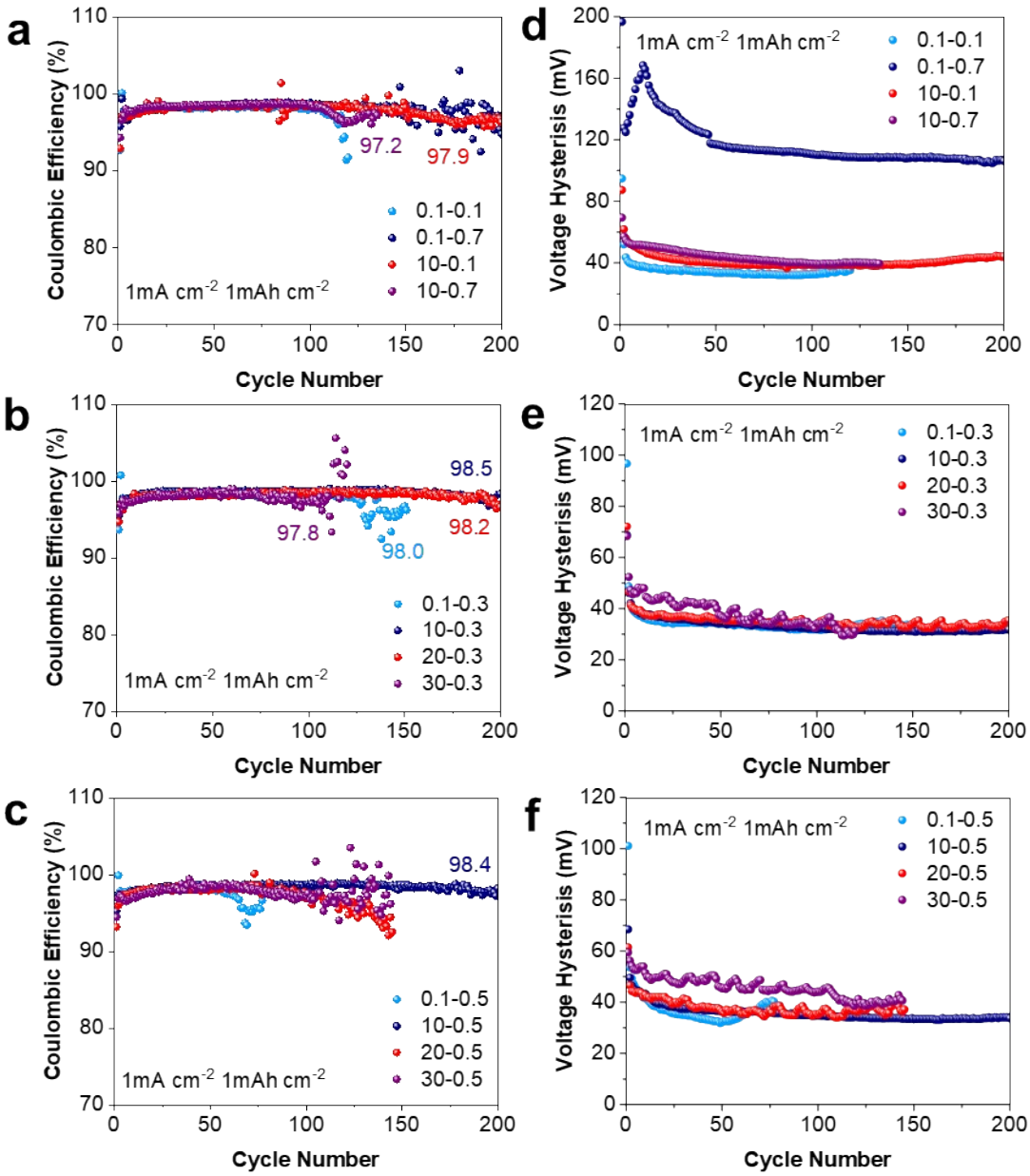


Figure S14. Electrochemical performances of Li||Cu cells with various formation strategies. (a-c) Comparison of the Li plating/stripping Coulombic efficiency (CEs) in Li||Cu cells at 1 mA $cm^{-2}$-1 mAh $cm^{-2}$, which were plated at the current density of 0.1 mA $cm^{-2}$ ~20 mA $cm^{-2}$ with the areal capacity of 0.1~0.7 mAh $cm^{-2}$, and corresponding (d-e) Voltage hysteresis.

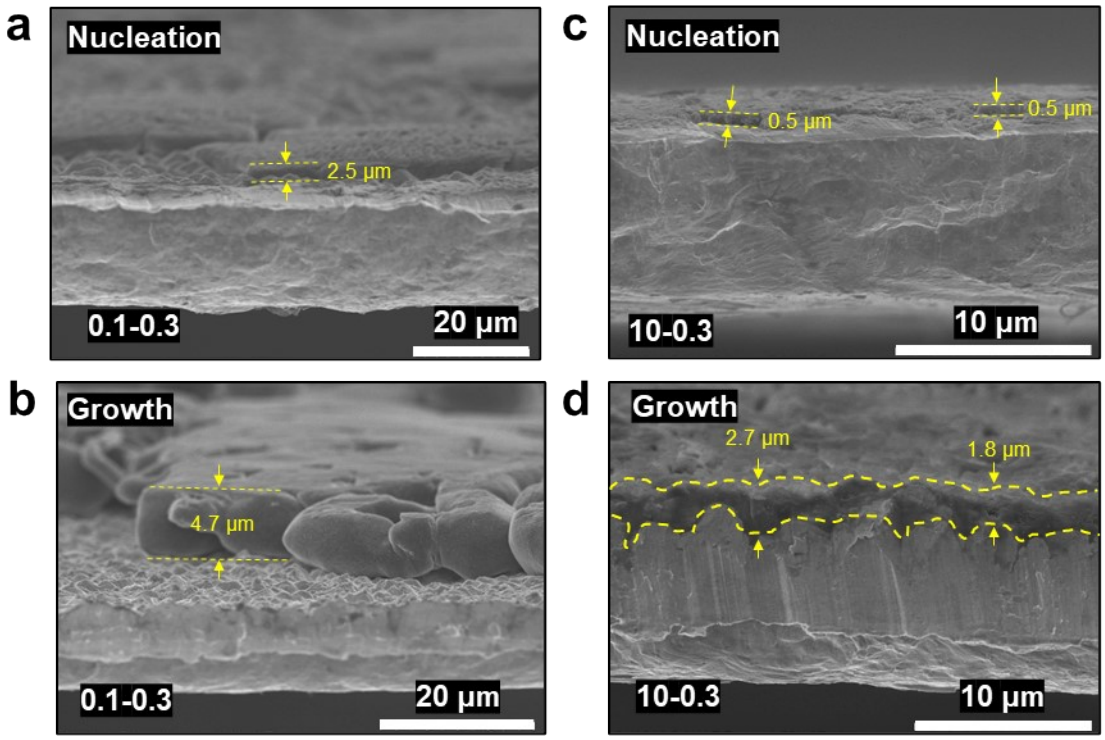


Figure S15. SEM images of Li nucleation and growth morphology of 0.1-0.3 and 10-0.3 cells cycled at 1 mA $cm^{-2}$, 1 mAh $cm^{-2}$ (The first deposition).

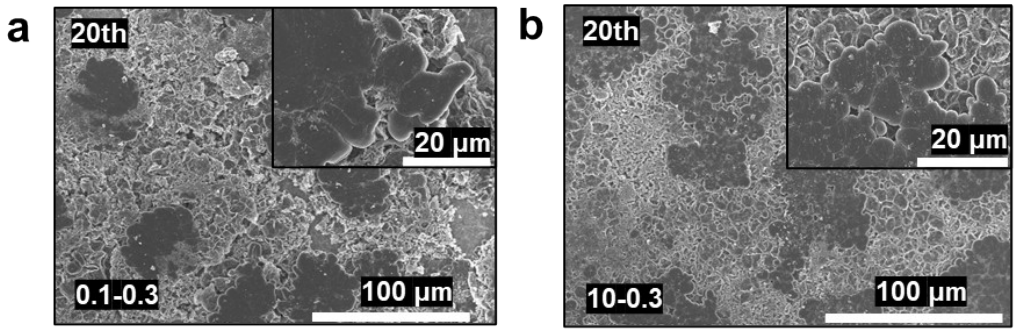


Figure S16. SEM images of Li deposit morphology of 0.1-0.3 and 10-0.3 cells cycled at 1 mA $cm^{-2}$, 1 mAh $cm^{-2}$. (After 20 cycles)

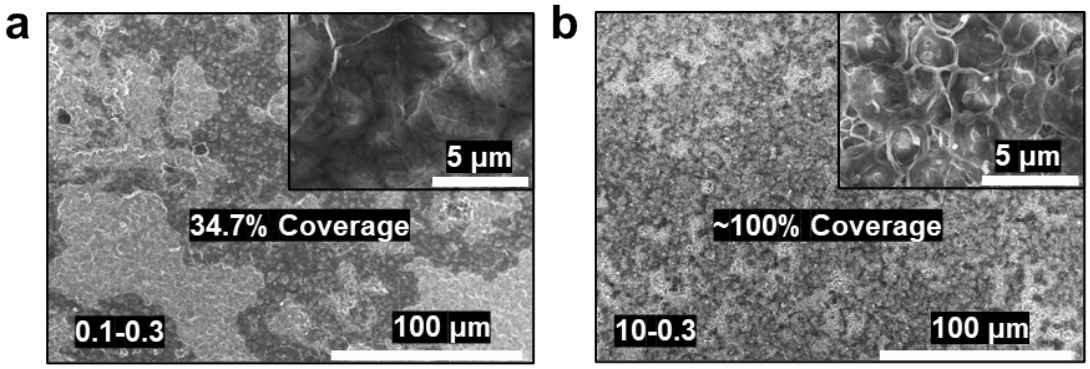


Figure S17. SEM images of the top view of Cu current collector after 1st Li striping in (a)0.1-0.3 and (b)10-0.3 cells cycled at 1 mA $cm^{-2}$, 1 mAh $cm^{-2}$.

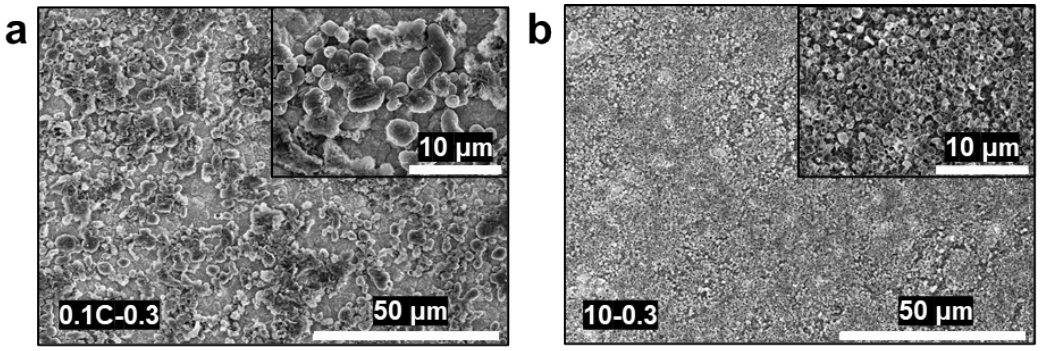


Figure S18. Morphologies of Li deposition on Cu current collectors in Cu||LFP anode-free cells with deposition capacity of 0.3 mAh $cm^{-2}$ at the current density of (a) 0.1C (~0.16 mA $cm^{-2}$) and (b) 10 mA $cm^{-2}$.

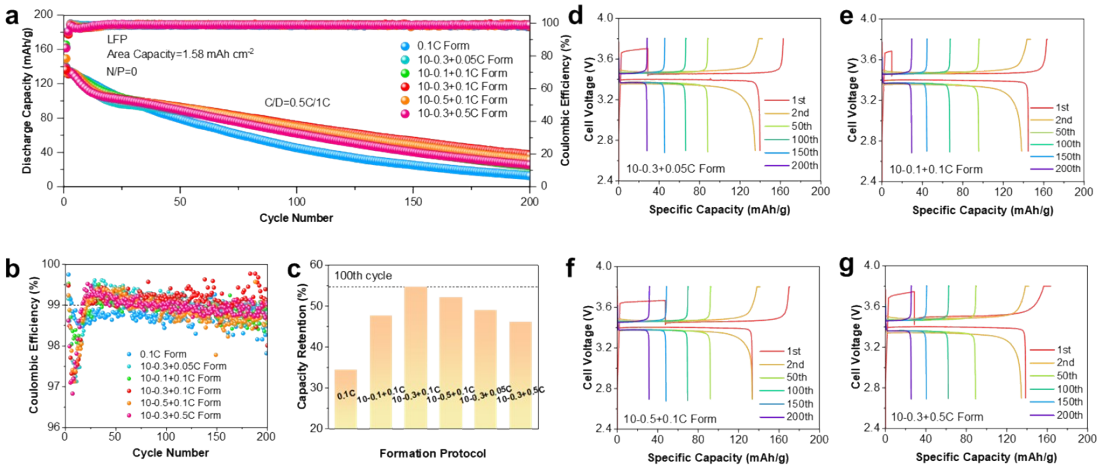


Figure S19. Electrochemical performance of Cu||LFP anode-free cells without or with high-current initiated formation strategy: 0.1C Form; 10-0.3+0.05C Form; 10-0.1+0.1C Form; 10-0.3+0.1C Form; 10-0.5+0.1C Form; 10-0.3+0.5C Form (Electrolyte for all tests was 1 M LiTFSI in DOL/DME (volume ratio 1/1) with 2 wt% $LiNO_3$.) (a) Cycling performance. (b) Coulombic efficiency. (c) Comparison of capacity retention after 100 cycles. (d-g) Galvanostatic charge–discharge curves with various formation strategies.

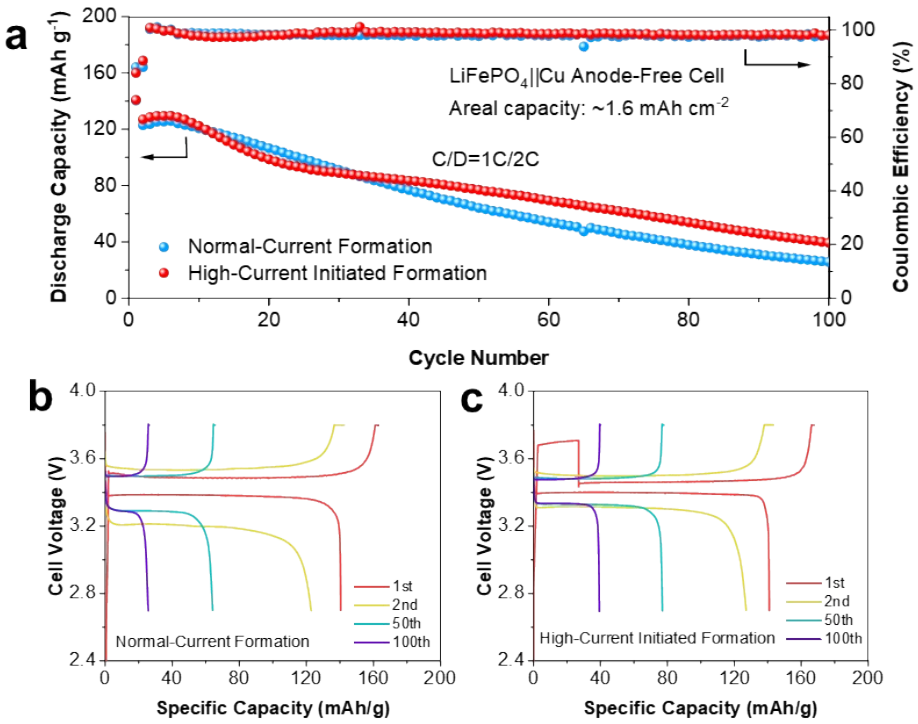


Figure S20. Electrochemical performance of Cu||LFP anode-free cells without or with high-current initiated formation strategy (Electrolyte for all tests was 1 M LiTFSI in DOL/DME (volume ratio 1/1) with 2 wt% $LiNO_3$.) (a) Cycling performance. (b-c) Galvanostatic charge–discharge curves with various formation strategies.

Table S1 Coulombic efficiency (CE) of high-current initiated formation strategy compared with other reported results.

| Cathode /Areal Capacity (mAh $cm^{-2}$) | Electrolyte | C/D Rate | Cycle Number | Capacity Retention (%) | C.E (%) | References |
|---|---|---|---|---|---|---|
| LFP/1.6 | 3 M LiFSI in DME/DOL (1:1, v/v) | 0.5mA $cm^{-2}$ | 100 | 40 | 98.78 | Concentrated salt and resting protocol, 2019[1] |
| NCM622/3.5 | [P1222][FSI] LiFSI (1:1, mol:mol) | 0.5C | 50 | 55.5 | 99.15 | Ionic liquid electrolyte and fast formation protocol, 2021[2] |
| LFP/1.4 | 1.6 M LiFSI in DME/TTE (v/v 1:4) | 1/3C | 100 | 41.5 | / | Potential hold method, 2022[3] |
| LFP/2.7 | 1.5M LiFSI in DME/HFE/DOL (0.8/1/0.2, vol.%) | 1mA $cm^{-2}$ 2mA $cm^{-2}$ | 100 | 51.0 | 99.4 (Within 50-100 cycle) | Dynamic galvanic corrosion, 2023[4] |
| LFP/2 | 1 M LiFSI in DME:TTE (1/2, vol.%) | 1mA $cm^{-2}$ 0.5mA $cm^{-2}$ | 100 | 38.3 | / | P-stripping strategy, 2023[5] |
| LFP/1.5 | 1 M LiTFSI in DOL/DME+2wt% $LiNO_3$ | 0.5C/1C | 50<br>100 | 70.8<br>54.7 | 98.7<br>99.0 | This work |

Table S2 Cell parameters of the anode-free pouch cell.

| Cell component | Parameter | Value |
|---|---|---|
| LFP Cathode (including Al foil) | Reversible capacity | 150 mAh $g^{-1}$ |
| | Active material loading | 91.5% |
| | Arial weight | 11.9 mg $cm^{-2}$ |
| | Area capacity | 1.6 mAh $cm^{-2}$ |
| | Electrode length | 80 mm |
| | Electrode width | 56 mm |
| | Thickness of Al foil | 20 μm |
| | Number of layers | 1 |
| Cu foil | Thickness | 12 μm |
| | Number of layers | 1 |
| Separator | Thickness | 16 μm |
| Electrolyte | Volume | 0.5 mL |
| Pouch cell | Length | 100 mm |
| | Width | 80 mm |
| | Total capacity | ~71 mAh |

# Supporting reference


1. T. T. Beyene, B. A. Jote, Z. T. Wondimkun, B. W. Olbassa, C.-J. Huang, B. Thirumalraj, C.-H. Wang, W.-N. Su, H. Dai and B.-J. Hwang, *ACS Applied Materials & Interfaces*, 2019, **11**, 31962-31971.
2. T. Pathirana, D. A. Rakov, F. Chen, M. Forsyth, R. Kerr and P. C. Howlett, *ACS Applied Energy Materials*, 2021, **4**, 6399-6407.
3. W. Shin and A. Manthiram, *Angewandte Chemie International Edition*, 2022, **61**, e202115909.
4. J.-F. Ding, R. Xu, Y. Xiao, S. Zhang, T.-L. Song, C. Yan and J.-Q. Huang, *Advanced Energy Materials*, 2023, **13**, 2204305.
5. Y. Xiao, R. Xu, L. Xu, Y.-X. Zhan, J.-F. Ding, S. Zhang, Z.-H. Li, C. Yan and J.-Q. Huang, *Advanced Energy Materials*, 2023, **13**, 2300959.